MESOSCOPIC STUDY OF TEXTILE REINFORCED COMPOSITES

M. Šejnoha[1*], J. Vorel[1], O. Jiroušek[2]

[1]*CTU in Prague, Faculty of Civil Engineering, Department of Mechanics, Thákurova 7, 166 29 Prague 6, Czech Republic*
[2]*Institute of Theoretical and Applied Mechanics, Academy of Science, Prosecká 809/76, 190 00 Prague 9, Czech Republic*
**e-mail address: sejnom@fsv.cvut.cz*

Keywords: Multi-scale, homogenization, SEPUC, XFEM, Mori-Tanaka, textile reinforced composites

Abstract
The present paper describes a two-step homogenization for the evaluation of effective elastic properties of textile reinforced composites. Attention is devoted to carbon and polysiloxane matrix based composites reinforced by plain weave textile fabrics. X-ray microtomography as well as standard image analysis are adopted to estimate the volume fraction, shape and distribution of major porosity, considerably influencing the resulting macroscopic response. Numerical procedure effectively combines the Mori-Tanaka averaging scheme and finite element simulation carried out on a suitable statistically equivalent periodic unit cell. Computational strategy employs the popular extended finite element method to avoid difficulties associated with meshing relatively complex geometries on the meso-scale. Comparison with the results obtained directly from the finite element simulations of available Micro-CT scans is also provided.

1 Introduction

Low out-of-plane stiffness of unidirectional fibrous composites together with the need for manufacturing sufficiently thick structural units considerably contributed to the introduction of more complex three-dimensional fiber preforms. This ushers in the subject of woven textile composites. While practical application of these material systems has a rich history, computational modeling of textile reinforced composites has witnessed a considerable activity only recently, see e.g. [1, 2] for an initiative work in numerical as well as analytical homogenization.

Regardless of the processing route these systems exhibit complex microstructures with a relatively large intrinsic porosity and a number of other fabrication related imperfections including non-uniform layer widths, tow undulation, inter-layer shift and nesting. Their accurate representation then calls for the development of sufficiently accurate geometrical models capturing reality as close as possible yet being computationally feasible. This requirement spans all relevant scales fitting textile composites well within the concept of hierarchical modeling. Starting from a simple one-layer computational model proposed in [3] several advances have been suggested leading to the concept of Statistically Equivalent Periodic Unit Cell (SEPUC) [4]. In contrast with traditional approaches, where parameters of the unit cell model are directly measured from available material samples, the SEPUC

approach is based on their statistical characterization. Being aware of various deficiencies of a single layer SEPUC [5] the authors developed in [6] a two-layer model capable of addressing most of the above irregularities. Discrete modeling of intrinsic discontinuities such as intra-yarn matrix cracks [7] or large inter-tow vacuoles (crimp voids) [6] then becomes relatively simple. Difficulties associated with the finite element discretization of the resulting computational model promoted the introduction of XFEM methodology (Extended Finite Element Method), typically used for the modeling of strong discontinuities, into the field of homogenization [8]. This allows for a considerable simplification in the preparation of finite element meshes which are then regular and do not have to confirm to actual material boundaries. Application of this strategy to textile composites is available, e.g. in [9, 6]. Apart from numerical approach usually based on the first-order homogenization the literature offers a number of analytical methods. The Mori-Tanaka method in particular gained a considerable interest owing to its simplicity and explicit format. Examples of successful application of this method to the evaluation effective thermal or elastic properties of imperfect textile composites can be found in [10, 11].

Effective combination of analytical and numerical techniques in the framework of multi-scale or hierarchical modeling then presents a vital tool for the analysis of such complex systems. Further advancement is expected when incorporating details of actual microstructure into the formulation of a computational model. A promising route can be seen in exploiting information provided by computer microtomography (μCT) [12]. Connecting the latter tool, either directly [13] or indirectly [14], with the previously mentioned approaches will become the principal objective of this paper. Liming our attention to carbon-carbon (C/C) textile composites we organize the paper as follows. Section 2 gives a brief introduction to principals of μCT. Basic steps associated with the application of XFEM in the light of first-order homogenization are outlined in Section 3. An illustrative example devoted to the derivation of effective thermal conductivities is presented in Section 4 followed by several concluding remarks in Section 5.

2 Computer microtomography

In the present study the computer microtomography is employed to derive an accurate three-dimensional map of meso-scale porosity accounting only for large inter-tow vacuoles. Intra-yarn matrix cracks, the major contributor to yarn porosity, are reflected in the prediction of tow effective properties from an independent homogenization step on the micro-scale. This step has been discussed in detail, e.g. in [6] and will not be repeated. Instead, we concentrate on meso-scale porosity only and examine two options of introducing this phase in numerical predictions. The first option considers the volume fraction only, whereas the second approach directly exploits the digitized model of a large sample of C/C textile developed from μCT images.

The experimental setup used in the present study consists of large-area flat panel sensor and microfocus X-ray source. Microfocus X-ray source L8601-01 (Hamamatsu Photonics K.K.) with tungsten anode, 5 μm spot size was used. For imaging, the C7942CA-22 X-ray detector (Hamamatsu Photonics K.K.) with the resolution of 2368x2240 pixels and physical dimensions of 120x120 mm was used; 2x2 pixel binning was adopted to reduce the acquisition time. The scanning sequence consisted of 720 scans with 0.5^0 step. Acquisition was performed using 10 times 0.5 s, voltage 80 kV and current 125 μA (the maximum setting of the power supply). The voltage/current ratio was set to produce the maximum signal to noise ratio in the radiographs.

A spatial resolution of the resulting 3D images was 12 μm^3. A particular example of 3D image of major porosity, amounting to 11% for the carbonized (CICIC) sample, is presented in Figure 1. It is clear that these estimates are crucially dependent on the voxel resolution with respect to the pore size. Nevertheless, if considering the volume of an average pore equal to 100 μm^3 and accept the error of one voxel for each edge of the pore (a rectangular parallelepiped is assumed for simplicity), the error induced by calculation of the volume fraction of pores is less than 7%. Thus for the carbonized sample the error (0.07x11% = 0.77%) will not exceed 1% of the total volume.

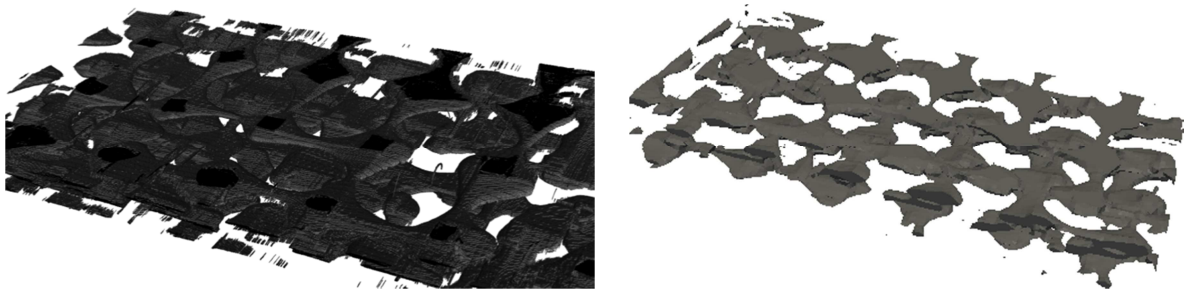

(a) (b)

Figure 1. Porous phase: a) Reconstructed CT scan; b) XFEM representation

3 Computational homogenization based on XFEM

First-order homogenization approach is adopted to estimate effective thermal conductivities as one particular example. Providing the composite is loaded by a macroscopically uniform temperature gradient $\boldsymbol{H}$ we derive the effective properties from the Hill lemma written as

$$\langle \delta \boldsymbol{h}(\boldsymbol{x})^{\mathrm{T}} \boldsymbol{\chi}(\boldsymbol{x}) \boldsymbol{h}(\boldsymbol{x}) \rangle = \mathbf{0}, \tag{1}$$

where $\boldsymbol{h}(\boldsymbol{x})$ is the local temperature gradient, $\boldsymbol{\chi}(\boldsymbol{x})$ represents the 3x3 conductivity matrix evaluated at a given point x and angular brackets stand for the volume averaging. In this context, the local temperature $\theta(\boldsymbol{x})$ admits the following decomposition

$$\theta(\boldsymbol{x}) = \mathbf{H} \cdot \boldsymbol{x} + \theta^*(\boldsymbol{x}), \tag{2}$$

where $\theta^*(\boldsymbol{x})$ corresponds to the fluctuation part of $\theta(\boldsymbol{x})$ and is assumed periodic (the same values of $\theta^*(\boldsymbol{x})$ are enforced on opposite sides of a rectangular periodic unit cell). With reference to standard finite element discretization the local temperature gradient is expressed in terms of nodal fluctuation temperatures as

$$\boldsymbol{h}(\boldsymbol{x}) = \boldsymbol{H} + \boldsymbol{B}(\boldsymbol{x}) \boldsymbol{\theta}_{\mathrm{d}}^*, \tag{3}$$

which upon substitution into Eq. (1) gives

$$\delta \boldsymbol{\theta}_{\mathrm{d}}^{*\mathrm{T}} \langle \mathbf{B}(\boldsymbol{X})^{\mathrm{T}} \boldsymbol{\chi}(\boldsymbol{X}) \mathbf{B}(\boldsymbol{X}) \rangle \boldsymbol{\theta}_{\mathrm{d}}^* = -\delta \boldsymbol{\theta}_{\mathrm{d}}^{*\mathrm{T}} \langle \mathbf{B}(\boldsymbol{X})^{\mathrm{T}} \boldsymbol{\chi}(\boldsymbol{X}) \rangle \boldsymbol{H}. \tag{4}$$

Once fluctuation temperatures are know they can be substituted back into Eq. (3) to provide the macroscopic heat flux $\boldsymbol{Q}$ in the form

$$\boldsymbol{Q} = \langle \mathbf{T}(\boldsymbol{x})^{\mathrm{T}} \boldsymbol{q}(\boldsymbol{x}) \rangle = -\frac{1}{|\Omega|} \int_{\Omega} \mathbf{T}(\boldsymbol{x})^{\mathrm{T}} \boldsymbol{\chi}(\boldsymbol{x}) \mathbf{T}(\boldsymbol{x}) \boldsymbol{h}(\boldsymbol{x}) \mathrm{d}\Omega \,, \tag{5}$$

where $\boldsymbol{q}(\boldsymbol{x})$ is the local heat flux and the transformation matrix $\mathbf{T}(\boldsymbol{x})$ is introduced to give the relationship between material matrices in the local and global coordinate systems as

$$\boldsymbol{\chi}(\boldsymbol{x}) = \mathbf{T}(\boldsymbol{x})^{\mathrm{T}}\boldsymbol{\chi}(\boldsymbol{x})\mathbf{T}(\boldsymbol{x}). \tag{6}$$

The result of Eq. (5) finally renders the macroscopic constitutive law

$$\boldsymbol{Q} = -\boldsymbol{\chi}^{\mathrm{H}}\boldsymbol{H}, \tag{7}$$

where $\boldsymbol{\chi}^{\mathrm{H}}$ is the searched 3x3 macroscopic homogenized conductivity matrix.

To avoid complications associated with standard meshing (FE mesh complies with all material boundaries) of complex geometries of textile composites further polluted by the porous phase we adopt the approach based on the extended finite element method. This method enables an application of regular meshes, which do not have to confirm to physical boundaries. These are captured by enriching the approximation space of the finite element with embedded interface exploiting the partition of unity technique. In the present context, theoretical formulation described by Möes et al. [8] is pursued.

The principal idea of XFEM is to augment the standard approximation space of temperatures with a specific enrichment function $\psi(\boldsymbol{x})$, which renders the corresponding gradients discontinuous along the material interface. Following [8], the augmented approximation of the temperature field reads

$$\theta(\boldsymbol{x}) = \sum_{i=1}^{I} N_i(\boldsymbol{x})\theta_i + \sum_{k=1}^{K}\sum_{j\in J_k} N_j^*(\boldsymbol{x})\psi(\boldsymbol{x})^k a_j^k, \tag{8}$$

where N_i are the standard shape functions, N_j^* are the shape functions building the local partition of unity, K stands for the number of enrichment functions (number of discontinuities within a single element), J_k gives the number of nodes for which the support is split by the discontinuity k and a_j^k are the additional degrees of freedom to approximate a zero-value level set function. Further details can be found in [6]. Two computational strategies employing the presented theoretical grounds will be now outlined.

3.1 Analysis based on SEPUC

The first approach builds upon existence of a certain Statistically Equivalent Periodic Unit Cell (SEPUC) derived by matching selected material statistics of a real composite sample and an artificial computational model.

In our previous work [5, 6] we proposed a two-layer SEPUC schematically displayed in Figure 2(a), where individual dimensions were subjected to optimization [6]. A two layer model is displayed in Figure 2(b). XFEM representations of individual fiber tows and porosity phase, clearly identifying material interfaces, are plotted in Figures 2(c,d). While fiber tows are directly related to an optimal two-layer model free of pores (Figure 2(b)), the porous phase is found subsequently by coating each fiber tow with a layer of matrix such that the volume of coating complies with the respective volume fraction of the matrix phase. The remaining space of the total volume of SEPUC then devolves upon the porous phase.

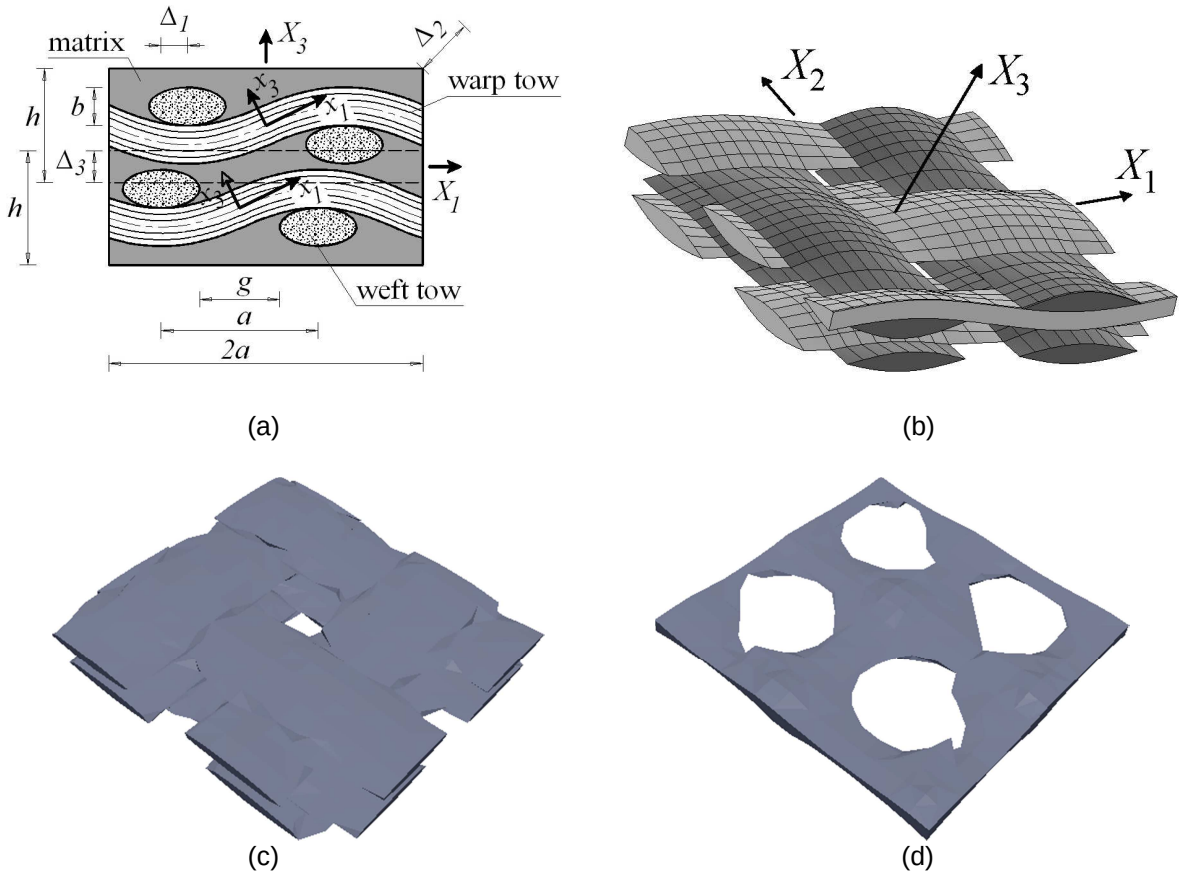

Figure 2. SEPUC: a) two dimensional cut; b) two-layer model including a periodic extension of an upper layer, c) XFEM representation of fiber tows, d) XFEM representation of porosity

3.2 Analysis based on data provides by μCT

The second approach considers direct exploitation of data provided by computational microtomography. Although visually distinguishable, see Figure 3, we still experienced considerable difficulties in discriminating between the fiber tows and the matrix phase numerically. Therefore, we accorded our attention to the porous phase only and substituted the tow-matrix composite by a homogeneous material with effective properties derived from an independent homogenization step using a modified SEPUC from Figure 2 free of pores.

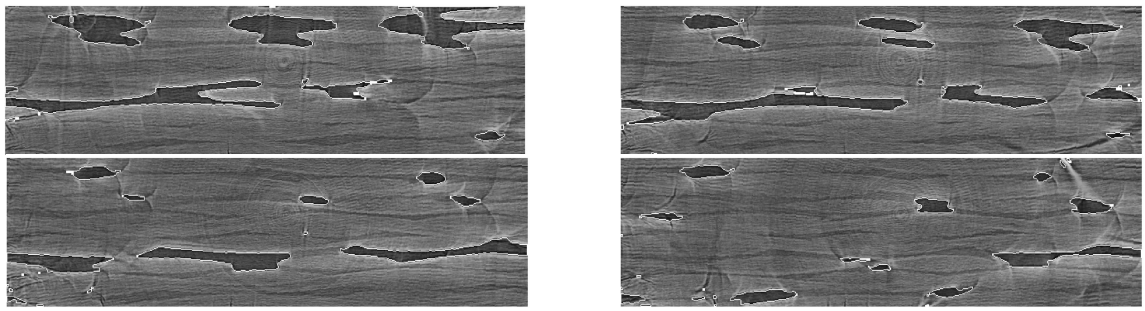

Figure 3. Position of pores given by image segmentation (four illustrative 2D cuts)

Nevertheless, this step still required additional segmentation of μCT data (Figure 3) to properly identify the shape and position of real pores. The corresponding XFEM representation then appears in Figure 4. Note that the black region represents the porous

phase. Further comparison is provided in Figure 1. It is clear that XFEM is able to represent the real porosity rather well.

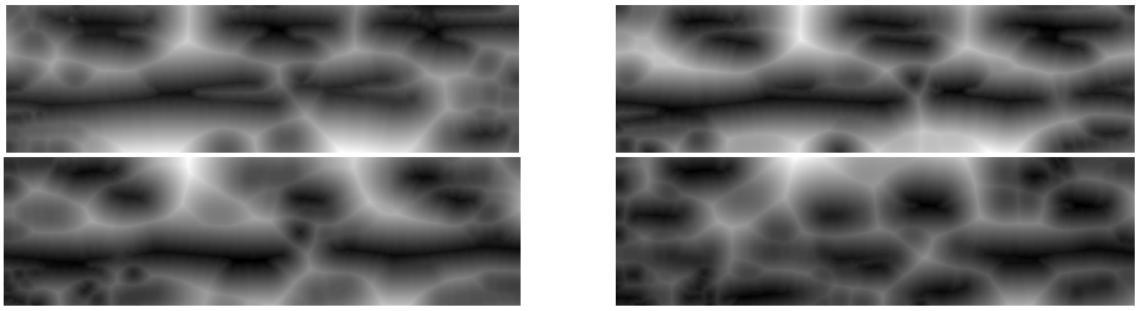

Figure 4. Level set function of real pores determined from 3D image of μCT scan (black = pores)

4 Numerical simulations

A comparative study of the two approaches discussed previously is presented in this section. Both strategies assume the same material properties listed in Table 1. It should be mentioned that the effective yarn properties are expected to be known. In this particular study these were found from an independent homogenization step. For simplicity we treated the fiber tow as another three-phase medium consisting of a unidirectional fiber-matrix composite weakened by longitudinal pores. This simplification invited an application of a simple Mori-Tanaka micromechanical model [10, 11]. Owing to some unpleasant features of the Mori-Tanaka method on the one hand and to reflect a significant size difference between fibers and pores on the other hand we performed the analysis in two independent steps. The fiber-matrix composite with circular fibers was considered first, followed by the second homogenization step of a porous medium with longitudinal pores having an elliptical cross-section embedded into the new effective matrix.

material	**conductivity [W/mK]**
matrix	6.3
yarn	24.12; 1.05; 1.42
air	0.02

Table 1. Thermal conductivities of individual constituents

In the light of the first order periodic homogenization the results pertinent to SEPUC are obtained directly from Eqs. (5) and (7) when running a steady state analysis for three loading cases with one component of $\boldsymbol{H}$ set equal to one while the other to zero. The volume flux averages, Eq. (5), then furnish the corresponding columns of the homogenized matrix $\boldsymbol{\chi}^{\mathrm{H}}$. The resulting effective conductivities for SEPUC dimensions stored in Table 2 are available in the last row of Table 3.

a	**b**	**g**	**h**	$\Delta x_{1,2}$	Δx_3
2181	118	422	251	333	20

Table 2. Dimensions of SEPUC [μm]

The results corresponding to the second approach are labeled as A1, A2 and B1, B2-1, respectively, to recognize the two step homogenization already mentioned in the previous section. Recall that in order to predict the resulting effective properties (A2, B2-1), we considered a real distribution of pores (provided by the μCT analysis) in an orthotropic, but

homogeneous, matrix. Properties of this matrix were estimated first from XFEM homogenization carried out at the level of SEPUC augmented by excluding the meso-scale porosity (A1). The second option involved the Mori-Tanaka method applied to an optimal single layer textile composite without porosity (B1), see [12] for details. For simplicity, periodic boundary conditions were adopted also in the second homogenization step (XFEM analysis of a porous sample). Since lacking geometrical periodicity, perhaps more appropriate approach would be to assume vanishing temperature fluctuations on the sample boundaries, thus providing an apparent upper bound on effective properties as discussed in [13].

For additional comparison we also offer the predictions provided solely by the Mori-Tanaka method (steps B1 and B2-2).

method	**volume fractions**			**conductivity [W/mK]**
	matrix	**yarns**	**pores**	
A1. XFEM without air voids (1st step)	0.531	0.469	-	9.08; 9.08; 2.94
A2. XFEM with real air voids (2nd step)	0.885		0.115	7.68; 7.67; 2.18
B1. MT without air voids (1st step)	0.531	0.469	-	9.16; 9.16; 2.69
B2-1. XFEM with real air voids (2nd step)	0.885		0.115	7.74; 7.72; 2.01
B2-2. MT with pores (2nd step)	0.885		0.115	7.75; 7.75; 2.20
XFEM for SEPUC	0.470	0.415	0.115	8.07; 8.07; 1.54

Table 3. Effective thermal conductivities

5 Conclusions

Two possible approaches for the derivation of effective properties of imperfect textile composites were briefly described. Both approaches rely on the solution of a homogenization problem with the help of XFEM methodology. The results provided by standard analysis of a periodic unit are corroborated by the results derived from large porous sample of a real composite, which allows us to account for complicated morphology of meso-scale porosity in a very accurate manner. Despite the fact that voxel representation of actual textile reinforcement was not adopted, we may still conclude that statistically equivalent representation of real material via SEPUC offers sufficiently accurate predictions. In this regard, the Mori-Tanaka method performed surprisingly well. Thus gaining sufficient confidence, the last two homogenization techniques will be exercised in our future study to also polysiloxane matrix based ceramic composites with several types of textile reinforcements.

Acknowledgement

The financial support provided by the GACR grant No. 105/11/0224 is gratefully acknowledged.

References

[1] Whitcomb J., K. Sriregan H. Effect of various approximations on predicted progressive failure in plain weave composites. *Composite Structures* **34(**1), pp. 13–20 (1996).
[2] Gommers B., Verpoest I., Van~Houtte P. The Mori-Tanaka method applied to textile composite materials. *Acta Materialia* **46(6),** pp. 2223–2235 (1998).
[3] Kuhn J. L., Charalambides P. G. Modeling of Plain Weave Fabric Composite Geometry. *Journal of Composite Materials* 33(3), pp.188–220 (1999).

[4] Zeman J., Šejnoha M. From random microstructures to representative volume elements. *Modelling and Simulation in Materials Science and Engineering* **15** (4), S325–S335 (2007).
[5] Zeman J., Šejnoha M. Homogenization of balanced plain weave composites with imperfect microstructure: Part I–Theoretical formulation. *International Journal of Solids and Structures* **41**(22-23), pp. 6549–6571 (2004).
[6] Vorel J., Zeman J., Šejnoha M. Homogenization of plain weave composites with imperfect microstructure: Part II–Analysis of real-world materials. *International Journal for Multiscale Computational Engineering*, In print (2012).
[7] Herb V., Couegnat G., Martin E. Damage assessment of thin SiC/SiC composite plates subjected to quasi-static indentation loading. *Composites: Part A* **41**, pp. 1766–1685 (2010).
[8] Möes N., Cloirec M., Cartraud P., Remacle J.-F. A computational approach to handle complex microstructure geometries. *Computer Methods in Applied Mechanics and Engineering* **192**(28-30), pp. 3163–3177 (2003).
[9] Genet M., Ladevéze P., Lubineau G. Toward virtual ceramic composites. *Proceedings of the 17th International Conference on Composite Materials (ICCM17)*, Edinburgh, Scotland, 2009.
[10] Skoček J., Zeman J., Šejnoha M. Effective properties of Carbon-Carbon textile composites: application of the Mori-Tanaka method. *Modelling and Simulationin Materials Science and Engineering* **16**(8), paper No. 085002 (2008).
[11] Vorel J., Šejnoha M. Evaluation of homogenized thermal conductivities of imperfect carbon-carbon textile composites using the Mori-Tanaka method. *Structural Engineering and Mechanics* **33**(4), pp. 429–446 (2009).
[12] Vavřík D., Dammer J., Jakubek J., Jeon I., Jiroušek O., Kroupa M., Zlámal P. Advanced X-ray radiography and tomography in several engineering applications. *Section Nuclear Instruments and Methods in Physics Research A: Accelerators, Spectrometers, Detectors and Associated Equipment* **633** (SUPPL. 1), pp. S152–S155 (2011).
[13] Pahr D. H., Züsset P. K. Influence of boundary conditions on computed apparent elastic properties of cancellous bone, *Biomech Model Mechanobiol* **7**(6), pp. 463—476 (2008).
[14] Drach B., Drach A., Tsukrov I. Characterization and Statistical Modeling of Irregular Porosity in Carbon/Carbon Composites Based on X-Ray Microtomography Data. *Zeitschrift für Angewandte Mathematik und Mechanik*, Accepted (2012).